Technical Paper

Transactions of the Society of
Naval Architects of Korea
Vol. 28, No. 1, April 1991
大韓造船學會論文集
第28卷 第1號 1991年 4月

Ultimate Compressive Strength-Based Safety and Reliability Assessment of the Double Skin Upper Deck Structure

by

Jeom K. Paik*

壓縮最終強度를 기준으로한 二重甲板構造의 安全性 및 信賴性 評價

白 点 基*

ABSTRACT

A practical procedure for the ultimate compressive strength-based safety and reliability assessment of the double skin upper deck structure is described. The external compressive stress acting on the upper deck structure which is due to the still water and wave-induced sagging moment is approximately estimated by using the existing rule of-classification society. The ultimate compressive stress of double skin structure under the action of sagging moment is analyzed by using idealized structural unit method. Here an idealized plate element subjected to uniaxial load is formulated by idealizing the nonlinear behaviour of the actual element taking account of the initial imperfections in the form of initial deflection and welding residual stress. The interaction effect between the local and global failure in the structure is also taken into consideration. The accuracy of the present method is verified comparing with the present solution and the existing numerical and experimental results for unit member and welded box columns. The safety of the structure is evaluated using the concept of conventional central safety factor and the reliablity assessment is made by using Cornel's MVFOSM method. The present procedure is then applied to upper deck structure of double skin product oil carrier. The influence of the initial imperfections and the yield stress of the material on the safety and reliability of the structure is investigated.

要 約

본 연구에서는 壓縮最終強度를 기준으로 한 二重甲板構造의 실용적인 安全性및 信賴性 평가법을 제안한다. 이를 위하여 船體上甲板에 작용하는 壓縮應力은 기존의 선급규정에 의해 근사적으로 추

Manuscript received : July 21, 1990, revised manuscript received : November 1, 1990.

*Member, Dept of Naval Architecture, Pusan National University

정하며, 壓縮最終強度는 理想化構造要素法을 적용하여 해석한다. 初期처짐 및 殘留應力의 영향과 局部挫屈 및 全體挫屈의 相關效果를 고려한 理想化板要素를 정식화한다. 理想化板要素의 精度와 有用性은 單位 板部材및 상자형 熔接構造物에 대한 기존의 實驗結果 또는 有限要素解析結果와 비교하여 확인한다. 본 제안법을 二重船殼構造設計개념하에서 설계된 精油運搬船의 甲板構造의 安全性및 信賴性評價에 적용하고, 초기처짐, 殘留應力등의 영향과 高張力鋼을 사용한 경우의 효과등에 대해 고찰한다.

1. Introduction

Steel structures such as ship and offshore structures under the action of excessive loading exhibit local failures associated with buckling and yielding until they reach the ultimate limit state as a whole. Moreover since steel structures are constructed by heating process like welding, initial imperfections in the form of initial deflection and welding residual stress that give rise to serious effects on both stiffness and strength of the structure are always present in the real structural members.

In order to carry out a more reliable design of steel structures, it is very important to make an assessment of safety and reliability considering initial imperfections as well as the interaction effect between the local and global buckling.

Recently, with the increasing of the needs for the construction of the double skin tanker, an ultimate strength-based safety and reliability assessment for the new types of ship structure becomes of great interest.

In this respect, the present study attempts to establish a practical procedure for the ultimate strength-based safety and reliability assessment of the double skin upper deck structure which is subjected to longitudinal compressive stress due to the sagging moment.

The compressive stress acting on the upper deck structure is approximately estimated by using the existing rule of classification society. Also the ultimate compressive stress of the structure is analyzed by using idealized structural unit method(ISUM).

A model for the imperfect plate element is formulated. The tangential elastic stiffness matrix, the condition of ultimate limit state and the post-ultimate stiffness matrix of the plate element is analytically formulated taking account of the initial imperfections in the form of initial deflection and welding residual stress. The interaction effect between the local and global failure in the structure is also taken into consideration. The accuracy and efficiency of the theory is verified comparing with the present solution and the existing experimental result for rectangular plates and welded box column.

The safety of the structure is evaluated using the central safety factor, and the reliability index applying mean-value first-order second-moment method[1].

The present safety and reliability assessment procedure is then applied to the double skin upper deck structure of product oil carrier designed by Okamoto et. al.[2]. The influence of the initial deflection and yielding stress on the safety and reliability of the structure is investigated.

2. Outline of the Objective Double Skin Upper Deck Structure

Ship's upper deck structure is subjected to the compressive stress in the longitudinal direction when the sagging moment is applied. As a

result, the upper deck structure at the midship part may buckle since the maximum bending stress acts on this part.

The objective double skin upper deck structure has a similar geometry with the conventional double bottom structure. The structure is composed of inner and outer skin plate elements. The longitudinal girders which are usually stiffened by the vertical and horizontal stiffeners are arranged. For the present double skin upper deck structure, no transverse members are arranged.

In the present study, the ultimate strength analysis is performed by using idealized structural unit method. In this case, the large size plate member composing the double skin upper deck structure is chosen as an unit element.

3. Assessment of the Central Safety Factor and the Reliability Index of the Upper Deck Structure

3.1 Central Safety Factor

The central safety factor of the structure on the basis of the ultimate strength reads

$$r=\mu_u/\mu_e \tag{1}$$

where r : the central safety factor of the structure

μ_u : the average ultimate compressive stress

μ_e : the average external compressive stress,

Hart et. al.[3] suggests that the average value of the external stress becomes to be two thirds times of the estimated stress. Thus

$$\mu_e=2/3\sigma=2/3(\sigma_s+\sigma_w) \tag{2}$$

where, σ : the total estimated stress

σ_s : the still water bending stress

σ_w : the wave-induced bending stress

Also, σ_s and σ_w can be calculated by using the existing rule of the classification society, in which the present study employes the ABS rule [4].

For simplicity, the average value of the ultimate compressive stress is evaluated dividing the ultimate load by the total cross-sectional area of the double skin upper deck structure in the present study. Thus,

$$\mu_u=P_u/A_d \tag{3}$$

where P_u : the ultimate load

A_d : cross-sectional area of double skin upper deck structure.

Substituting Eqs. (2) and (3) into Eq. (1), the central safety factor r is given.

3.2 Reliability Index

Cornel's MVFOSM method[1] is employed for the assessment of the reliability index(or safety index) which is emerged by

$$\beta=\frac{\mu_u-\mu_s-\mu_w}{\sqrt{S_u^2+S_s^2+S_w^2}} \tag{4}$$

where β : the reliability index

μ_u : the average value of the ultimate compressive stress

μ_s : the average value of the still water bending stress

μ_w : the average value of the wave-induced bending stress

μ_u : the standard deviation of the ultimate compressive stress

μ_s : the standard deviation of the still water bending stress

μ_w : the standard deviation of the wave-induced bending stress

μ_s and μ_w in Eq.(4) are also evaluated by the simple method suggested by Hart et. al.[3]. Thus,

$$\mu_s=2/3\sigma_s$$
$$\mu_w=2/3\sigma_w \tag{5}$$

Also S_u ane S_s are calculated by using the

coefficient of variance for each variable as

$$S_u = COV_u \, \mu_u$$
$$S_s = COV_S \, \mu_S \quad (6)$$

where COV_u and COV_s denote the coefficients of variance for the ultimate stress and the still water bending stress, respectively.

Since the ultimate compressive stress and the still water bending stress are due to the action of the static loading, it is assumed that probability distribution has normal function.

On the other hand, the frequency distribution of the wave-induced stress becomes to be more complex. In this study, the probability distribution of the wave-induced stress is assumed to have the following exponential function.

$$F(\sigma_w) = 1 - \exp(\sigma_w/\lambda) \quad (7)$$

where λ : the scale parameter of the exponential function

σ_w : the estimated wave-induced bending stress

Thus the average value and the standard deviation of the wave-induced bending stress read

$$\mu_w = 2/3 \; \sigma_w = \lambda(\alpha + \ln N) \quad (8.a)$$
$$S_w = \pi\lambda/\sqrt{6} \quad (8.b)$$

where N : the number of wave encountered by the ship during the life time

α : Euler's constant($=0.5772$)

In Eq.(8), when considering that ship's life time is 20 years, the wave number N becomes to be 10^8. Also, λ is given from Eq.(8.a) once σ_w is known.

Thus substituting Eq.(5), (6) and (8) into Eq.(4), the reliability index β is obtained.

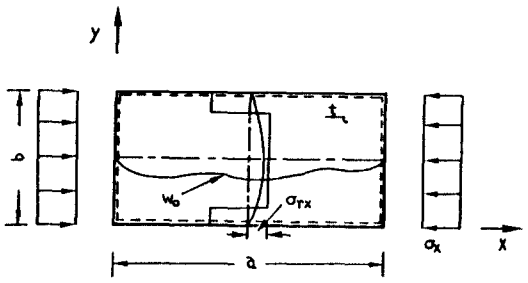

Fig.1 Configuration of the external loading and initial imperfections in the rectangular plate element

4. Analysis of Ultimate Compressive Stress of Double Skin Upper Deck Structure

4.1 Brief Description of Nonlinear Behaviour of a Plate Element

In this study, the idealized structural unit method is applied in order to analyze the ultimate compressive stress of double skin upper deck structure. Here, a large size plate member is chosen as an idealized plate element which is to be formulated by idealizing the nonlinear behaviour of the actual plate element in advance.

As shown in Fig.1., a dominant loading component acting on the local plate element under the consideration is the uniaxial compression. Also the plate has the initial imperfections in the form of initial deflection and welding residual stress.

As the external load increases, the deflection

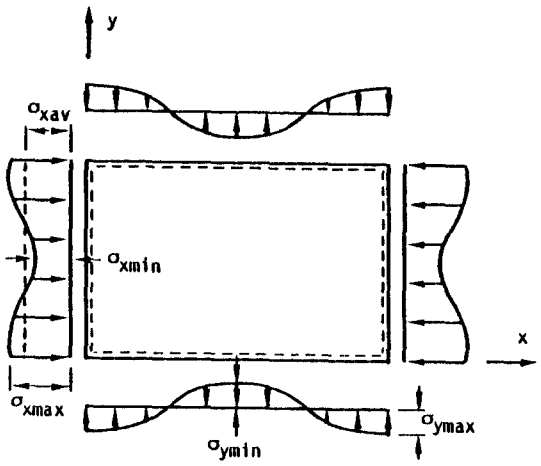

Fig.2 Membrane stress distribution of the deflected plate element subjected to uniaxial compression

of the plate gradually increases from the beginning in which a clear buckling phenomenon is not appeared. Also the inplane stiffness of the plate gradually decreases with the increasing of the load.

If the plate has a lateral deflection, the membrane stress distribution in the loading direction becomes to be non-uniform as shown in Fig.2. The maximum membrane stress is developed in the corner while minimum stress is appeared in the middle part. In actual, since the boundary condition of the plate element is supposed to be simply supported, in which the edges are considered to remain straight even after the lateral deflection is occured, the stress distribution in the transverse direction is also non-uniform. In this case the tensile stress is developed in the middle part and the compressive stress is appeared in the corner so as to achieve an self-equilibrium state in the transverse direction. The stress distribution may also depend on the existing of welding residual stress.

Therefore the middle part at the longitudinal edge of the plate under consideration is likely to be yielded rather than the corner. And if a plastic territory is formed at this part, the local plate may collapse since the membrane tension can not resist further against the increasing of the deflection [5]. Also if the welding residual stress is present in the plate, an earlier occurence of the plasticity is expected.

In the post-ultimate range of the plate, the force follows the unloading path although the deformation increases further.

4.2 Formulation of the Idealized Plate Element Subjected to Uniaxial Load

As mentioned in the previous section, the actual plate member has initial deflection and it gives rise to an serious effect to the elastic stiffness of the plate element. Also it is known that the global nonlinear behaviour of the whole structure seriously depends upon the local member's failure in the structure.

In this respect, a fomulation of the tangential elastic stiffness matrix is made taking account of the influence of initial imperfections as well as the interaction effect between the local and global failure in the structure. Here, the latter is taken into account by applying the large deformation theory on the basis of the updated Lagrangian formulation in a similar way of the conventional finite element method.

(1) Nodal Forces and Nodal Displacements of the Element

Since the bending stiffness of the plate element is considered to be small comparing with the inplane stiffness, the element is supposed to be negligible. Thus the behaviour of the present plate element is expressed by the nodal force vector{R} and displacement vector {U} having three degrees of freedom at each corner nodal point which is constructed in the mid-thickness as shown in Fig.3.

$$\{R\}=\{R_{x1}\ R_{y1}\ R_{z1}\ R_{x2}\ R_{y2}\ R_{z2}\ R_{x3}\ R_{y3}\ R_{z3}\ R_{x4}\ R_{y4}\ R_{z4}\}^T$$

$$\{U\}=\{u_1\ v_1\ w_1\ u_2\ v_2\ w_2\ u_3\ v_3\ w_3\ u_4\ v_4\ w_4\}^T \quad (9)$$

where R_x, R_y and R_z indicate axial forces in the x, y and z direction and also u, v and w represent displacements in the x, y and z direction, respectively.

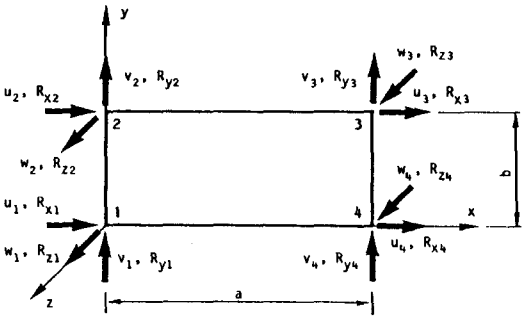

Fig.3 Nodal force and nodal displacement of an idealized plate element

(2) Strain-Displacement Relation

The relationship between the membrane stratin and displacement taking account of the large defornation effects of out-of-plane of the element reads

$$\varepsilon_x = u_{,x} + 1/2(w_{,x})^2$$
$$\varepsilon_y = v_{,y} + 1/2(w_{,y})^2 \quad (10)$$
$$r_{xy} = u_{,x} + v_{,y} + w_{,x}\, w_{,y}$$

where ε_x, ε_y and γ_{xy} indicate the membrane strain components for a plane stress state.

The incrimental expression of Eq.(10) is emerged by

$$\Delta\varepsilon_x = \Delta u_{,x} + w_{,x}\Delta w_{,x} + 1/2(\Delta w_{,x})^2$$
$$\Delta\varepsilon_y = \Delta v_{,y} + w_{,y}\Delta w_{,y} + 1/2(\Delta w_{,y})^2 \quad (11)$$
$$\Delta_{xy} = \Delta u_{,y} + \Delta v_{,x} + \Delta w_{,x}\Delta w_{,y} + w_{,x}\Delta w_{,y} + \Delta w_{,x}\Delta w_{,y}$$

where prefix Δ denotes the infinitesimal increment of each variable.

Since the nodal displacement vector {U} can be split into {S} and {W} which denote the in-plane and out－of－plane component of the vector {U}, respectively, Eq.(11) is rewritten by using the following matrix form.

$$\{\Delta\varepsilon\} = [B_0]\{\Delta S\} + [C][G]\{\Delta W\} + 1/2[\Delta C][G]\{\Delta W\} \quad (12)$$

where $\{\Delta\varepsilon\} = \{\Delta\varepsilon_x \Delta\varepsilon_y \Delta r_{xy}\}^T$

$\{U\} = \{S\ W\}$

$\{S\} = \{u_1 v_1 u_2 v_2 u_3 v_3 u_4 v_4\}^T$

$\{W\} = \{w_1\ w_2\ w_3\ w_4\}^T$

$[B_0]\{S\} = \{u_{,x}\ v_{,y}\ u_{,y} + v_{,x}\}^T$

$[G]\{W\} = \{w_{,x}\ w_{,y}\}^T$

$$[C] = \begin{bmatrix} w_{,x} & 0 \\ 0 & w_{,y} \\ w_{,y} & w_{,x} \end{bmatrix}$$

(3) Stress-Strain Relation of Deflected Plate Element in the Elastic Range

When the plate element has lateral deflection, membrane stress distribution becomes to be non-uniform with the increasing of the external force and then the in-plane stiffness of the element decreases.

The present theory attempts to treat the locally deflected plate element as the equivalent flat plate element taking account of the decrease of the in-plane stiffness.

The axial compression dominantly acts on the present plate element. The magnitude of the shear stress acting on the element is considered to be very small. Also, since the edges of the element are supposed to remain straight, the average strain component at the edges of the element reads[5]

$$\varepsilon_x = 1/E\ \sigma_{xmax} - \nu/E\ \sigma_y \quad (13.a)$$
$$\varepsilon_y = -\nu/E\ \sigma_X + 1/E\ \sigma_{ymax} \quad (13.b)$$
$$r_{xy} = 2(1+\nu)/E\ \tau_{xy}$$

where σ_{xmax}, σ_{ymax}, τ_{xy} : the maxixmum membrane stress components

σ_x, σ_y, τ_{xy} : the average membrane stress components

ε_x, ε_y, r_{xy} : the average atrain components

σ_{xmax} and σ_{ymax} in Eq.(13) is analytically derived in terms of σ_x and σ_y by solving the governing equation of deflected plate element subjected to uniaxial load. The maximum and minimum membrane stress components are then given by[5]

$$\sigma_{xmax} = \sigma_x + \sigma_{xL}$$
$$\sigma_{ymax} = \sigma_{yL} \quad (14.a)$$
$$\sigma_{xmin} = \sigma_x - \sigma_{xL}$$
$$\sigma_{ymin} = -\sigma_{yL} \quad (14.b)$$

where $\sigma_{xL} = Em^2\pi^2/8a^2 \cdot w_m(w_m + 2w_{om})$

$\sigma_{yL} = E\pi^2/8b^2 \cdot w_m(w_m + 2w_{om})$

σ_x, σ_y : the average membrane stress in the x and y direction

σ_{rx} : the compressive residual stress located in the center of the plate (see Fig.1)

m : the buckling wave number which is determined as integer satisfied by $a/b \leq \sqrt{m(m+1)}$

w_{om} : the initial deflection component

for the buckling wave number in the longitudinal direction of the element

w_m : the added deflection component for the buckling wave number in the longitudinal direction of the element which is obtained by

$$w_m = -c_2/3c_1 + k_1 + k_2$$

$$k_1 = \{-c_6/2 + (c_6^2/4 + c_5^3/27)^{1/2}\}^{1/3}$$

$$k_2 = \{-c_6/2 - (c_6^2/4 + c_5^3/27)^{1/2}\}^{1/3}$$

$$c_1 = E(m^4\pi^2/a^4 + \pi^2/b^4)$$

$$c_2 = 3w_{om}c_1$$

$$c_3 = 2w_{om}^2 c_1 + 4\pi^2 Et^2/3(1-\nu^2)(m^2/a + 1/b^2)^2 - 16\{m^2/a^2(\sigma_x + \sigma_{rx}) + 1/b^2\}$$

$$c_4 = -16w_{om}\{m^2/a^2(\sigma_x + \sigma_{rx}) + 1/b^2\}$$

$$c_5 = c_3/c_1 - c_2^2/3c_1^2$$

$$c_6 = 2c_2^2/27c_1^3 - c_2c_3/3c_1^2 + c_4/c_1$$

Substituting Eq.(14) into Eq.(13) and expressing it by an incremental form, the following stress-strain relation is emerged.

$$\{\Delta\sigma\} = [D]^E \{\Delta\varepsilon\} \quad (15)$$

where $[D]^E$: the stress-strain matrix of the deflected plate element in the elastic range.

(4) Shape Function

As mentioned in the previous section, since the bending stiffness of the element is supposed to be negligible and also the locally deflected plate element is treated as the equivalent flat plate element with the corresponding in-plane stiffness resulting from the existence of the lateral deflection, the following linear function is taken for the out-of-plane as well as the in-plane displacement function.

$$u = a_1 + a_2x + a_3y + a_4xy + b_4/2(b^2 - y^2) \quad (16.a)$$

$$v = b_1 + b_2x + b_3y + b_4xy + a_4/2(a^2 - x^2) \quad (16.b)$$

$$w = c_1 + c_2x + c_3y + c_4xy \quad (16.c)$$

where the last term at the right hand side of Eq. (16.a) and (16.b) is added such that the shear strain inside the element becomes to be uniform.

(5) Tangential Elastic Stiffness Matrix of the Plate Element

Applying the principle of the virtual work, the following equation should be satisfied.

$$\delta\{\Delta U\}^T\{R + \Delta R\} = \int_v \delta\{\Delta\varepsilon\}^T\{\sigma + \Delta\sigma\}dVol \quad (17)$$

where the left hand side term represents the external work done by the virtual displacement and the right hand side term indicates the strain energy stored during the acting of the virutal strain increment, in which prefix δ denotes the virtual value. Also $\int(\cdot)dvol$ denotes the integrating for the entire volume of the element.

The virtual strain increment $\delta\{\Delta\varepsilon\}$ is calculated by differentiating Eq.(12) with respect to the increment of the displacement component.

$$\delta\{\Delta\varepsilon\} = [B_o]\delta\{\Delta S\} + [C + \Delta C][G]\delta\{\Delta W\} \quad (18)$$

Substituting Eqs.(12), (15) and (18) into Eq. (17) and neglecting the higher order terms with respect to the increment, the following elastic stiffness equation of the element in the local coordinate is finally emerged.

$$\{L\} + \{\Delta R\} = [K]^E\{\Delta U\} \quad (19)$$

where,$[K]^E$: the tangential elastic stiffness matrix of the element

$\{L\} = \{R\} - \{r\}$: the unbalance force caused by the discrepancy between the total external force$\{R\}$ and the total internal force$\{r\}$

Also the total internal force$\{r\}$ in Eq.(19) is numerically calculated by

$$\{r\} = \int [B_o]^T\{\sigma\}dVol + \int [G]^T[C]^T\{\sigma\}dVol \quad (20)$$

where,$\{\sigma\} = \{\sigma_x \quad \sigma_y \quad \tau_{xy}\}$: the total average membrane stress components

By the way, the tangential stiffness matrix $[K]^E$ in Eq.(19) is split into the following three terms.

$$[K]^E = [K_o] + [K_G] + [K\sigma] \quad (21)$$

where $[K_o] = \begin{bmatrix} [K_1] & [O] \\ [O] & [O] \end{bmatrix}$

$$[K_G] = \begin{bmatrix} [O] & [K_2] \\ [K_2]^E & [K_3] \end{bmatrix}$$

$$[K\sigma] = \begin{bmatrix} [O] & [O] \\ [O] & [K_4] \end{bmatrix}$$

$$[K_1] = \int [B_o]^T [D]^E [B_o]\, dVol$$

$$[K_2] = \int [B_o]^T [D]^E [C] [G]\, dVol$$

$$[K_3] = \int [G]^T [C]^T [D]^E [C] [G] dVol$$

$$[K_4] = \int [G]^T [\sigma] [G]\, dVol$$

$$[\sigma] = \begin{bmatrix} \sigma_x & \tau_{xy} \\ \tau_{xy} & \sigma_y \end{bmatrix}$$

In the right hand side of Eq.(21), the first term $[K_o]$ indicates the stiffness matrix related to the small deformation. Also the second one $[K_G]$ which is called the initial deformation stiffness matrix represents the geometric nonlinear effect and the third term$[K\sigma]$, so called the initial stress stiffness matrix is produced by the existence of the initial stress.

The stiffness matrix in Eq.(21) was derived under the consideration that the local coordinate of the element is fixed with regard to the global space one, which makes possible to use the identical transformation matrix through every incremental loading steps.

On the other hand, using the concept of updated Lagrangian formulation in which the local coordinate may become to be altered and updated in each deformed state of the element such that the transformation matrix from the local and the global coordinate should be newly set up, the initial deformation matrix$[K_G]$ in Eq. (21) can be removed because the initial deformation in the beginning of each incremental loading step has become to be eliminated.

Thus the final form of the tangential elastic stiffness matrix of the element will be emerged by

$$[K]^E = [k_o] + [k_o] \qquad (22)$$

(6) Criterion of the Ultimate Limit State of Plate Element Subjected to Uniaxial Load

The initially deflected plate element exhibits no clear buckling phenomenon with the increasing of the external force because the lateral deflection gradually increases from the beginning. If the plasticity starts inside the element, then the in-plane stiffness of the element decreases and finally the plate will collapse.

The upper and/or lower surface at the center of the deflected plate is likely to be yielded rather than other place, but in actual although the plate center becomes to be yielded, the plate does not collapse in the case of relatively thin plates widely used in ship structures until the portion at edge is yielded.

The present element is subjected to uniaxial load and if the middle points at the longitudinal edge is yielded, the plate is considered to reach the ultimate limit state.

Therefore, by applying Mises's yieding condition, the condition of the formation of the plasticity at the middle point of the longitudinal edge reads

$$\Gamma_p = \sigma_{xmax}^2 - \sigma_{xmax}\,\sigma_{ymin} + \sigma_{ymin}^2 - \sigma_0^2 = 0 \qquad (23)$$

Substituting the maximum and/or minimum membrane stress components given in Eq.(14) into Eq.(23) and if the condition is satisfied, then the plate is considered to collapse.

(7) Derivation of the Post-Ultimate Stiffness Matrix of the Plate Element

In the post-ultimate range of the element, the internal stresses follow the unloading path even though the deformation continuously increases.

In general, for thin plates, it is assumed that the magnitude of the stress compoments at the yielded point is not changed so seriously. Thus, after the element collapses, the maximum membrane stress components at the yielded

point are supposed to remain constant in the subsequent loading step.

Therefore, just after the element reaches the ultimate limit state, the membrane stress components at the yielded point are numerically given by

$$\sigma_{xmax} = \sigma_{xmax}^{u}$$
$$\sigma_{ymax} = \sigma_{ymax}^{u} \quad (24)$$

where, superscript u indicates the value just after the element reaches the ultimate limit state.

The average membrane stress components of the element in the post-ultimate range are given by using the concept of the effective width[6].

$$\sigma_{xav} = b_e/b \cdot \sigma_{xmax}$$
$$\sigma_{yav} = a_e/a \cdot \sigma_{ymax} \quad (25)$$

where, b_e and a_e represent the effective widths in the longitudinal and transverse direction, respectively.

With the increasing of the deformation, the effective widths contineously decrease even in the post-ultimate range. Here, the reduction tendancy of the effective widths in the post-ultimate range is supposed to be same in the pre-ultimate range. Thus, the effective widths read

$$b_e/b = \sigma_{xav^*}/\sigma_{xmax^*}$$
$$a_e/a = \sigma_{yav^*}/\sigma_{ymax^*} \quad (26)$$

where σ_{xav^*}, σ_{yav^*} : the virtual average membrane stresses

σ_{xmax^*}, σ_{ymax^*} : the virtual maximum membrane stresses

Also, the asterisk indicates that the stress is a virtual value in the post-ultimate range.

Using Eq.(14), the virtual average membrane stresses are expressed in terms of the virtual maximum membrane stresses as

$$\{\sigma_{av^*}\} = [\sigma_m]^{-1}\{\sigma_{max^*}\} \quad (27)$$

where, $\{\sigma_{av^*}\} = \{\sigma_{xav^*}\ \sigma_{yav^*}\}^T$

$\{\sigma_{max^*}\} = \{\sigma_{xmax^*}\ \sigma_{ymax^*}\}^T$

$[\sigma_m]$: the maximum stress-average stress matrix which is numerically calculated in each loading step

The virtual maximum membrane stresses are calculated by using the average strain as

$$\{\sigma_{max^*}\} = [D_m]\{\varepsilon_{av}\} \quad (28)$$

where, $\{\varepsilon_{av}\} = \{\varepsilon_{xav}\ \varepsilon_{yav}\}^T$

$$[D_m] = \frac{E}{1-\nu^2}\begin{bmatrix} 1 & \nu \\ \nu & 1 \end{bmatrix}$$

Substituting Eqs.(27) and(28) into Eq.(26), the effective widths in the post-ultimate range are expressed in terms of the average strain as

$$b_e/b = [b_m]\{\varepsilon_{av}\}$$
$$a_e/a = [a_m]\{\varepsilon_{av}\} \quad (29)$$

where, $[b_m]$: longitudinal effective width-the average strain matrix

$[a_m]$: the transverse effective width-the average strain matrix

Again, by substituting Eqs.(24) and (29) into Eq.(25), the average membrane stresses are given

$$\sigma_{xav} = \sigma_{xmax}^{u} \cdot [b_m]\{\varepsilon_{av}\}$$
$$\sigma_{yav} = \sigma_{ymax}^{u} \cdot [a_m]\{\varepsilon_{av}\} \quad (30)$$

On the other hand, since the occurence of the shearing buckling is not expected in the present element, the shearing stiffness of the element is supposed to be fully effective even in the post-ultimate range. Thus, the same relation between the shearing stress and strain with Eq.(13.c) is employed.

Taking Eqs.(30) and (13.c) by the incremental form, the following stress-strain relation in the post-ultimate range is emerged.

$$\{\Delta\sigma\} = [D]^U\{\Delta\varepsilon\} \quad (31)$$

where, $[D]^U$: the post-ultimate stress-strain matrix

Consequently, the post-ultimate stiffness matrix of element is obtained by replacing $[D]^E$ in Eq.(22) with $[D]^u$ in Eq.(31).

4.3 Verification of the Present Theory

Table. 1 Description of the test specimen for the welded square plate subjected to uniaxial compression

Specimen No.	t(㎜)	σ_o (kg/㎟)	b/t	W_o/t	σ_{tx} (kg/㎟)	EXP.		THE.		K(%)
						σ_u	σ_u/σ_o	σ_u	σ_u/σ_o	
A－ 1	4.50	28.49	111.11	0.00	2.00	11.11	0.39	12.79	0.45	15.12
A－ 2	4.50	26.59	111.11	0.00	2.00	11.96	0.45	12.10	0.46	1.17
A－ 3	4.50	26.66	111.11	0.09	2.00	10.93	0.41	11.94	0.45	9.24
A－ 4	4.50	26.00	111.11	0.09	2.00	11.96	0.46	11.67	0.45	−2.42
A－ 5	4.50	25.87	111.11	0.09	2.00	11.64	0.45	11.67	0.45	0.26
A－ 6	4.50	26.27	111.11	0.24	2.00	11.56	0.44	11.51	0.44	−0.43
A－ 7	4.50	28.07	111.11	0.27	2.00	11.51	0.41	12.15	0.43	5.56
A－ 8	4.50	26.45	111.11	0.31	2.00	11.11	0.42	11.43	0.43	2.88
A－ 9	4.50	26.88	111.11	0.36	2.00	11.29	0.42	11.56	0.43	2.39
A－10	4.50	26.66	111.11	0.38	2.00	10.93	0.41	11.46	0.43	4.85
A－11	4.50	28.03	111.11	0.89	2.00	10.93	0.39	11.18	0.40	2.29
A－12	4.50	25.16	111.11	1.02	2.00	9.56	0.38	9.84	0.39	2.93
A－13	4.34	22.01	115.21	0.33	5.00	6.98	0.32	7.40	0.34	6.02
A－14	4.34	22.01	115.21	0.52	5.00	7.12	0.32	7.09	0.32	−0.42
A－15	4.34	23.42	115.21	1.07	5.00	7.05	0.30	6.84	0.29	−2.98
A－16	4.34	23.08	115.21	1.28	5.00	7.81	0.34	6.49	0.28	−16.90
A－17	4.34	21.05	115.21	1.31	5.00	7.28	0.35	5.75	0.27	−21.02
A－18	4.34	22.87	115.21	1.74	5.00	7.66	0.33	6.01	0.26	−21.54
B－ 1	8.80	31.03	56.82	0.00	2.00	27.00	0.87	24.48	0.79	−9.33
B－ 2	8.80	31.20	56.82	0.00	2.00	26.52	0.85	24.46	0.78	−7.77
B－ 3	8.80	31.06	56.82	0.00	2.00	28.89	0.93	24.48	0.79	−15.26
B－ 4	8.80	28.71	55.56	0.00	2.00	24.40	0.85	24.12	0.84	−1.15
B－ 5	8.80	31.96	56.82	0.26	2.00	21.73	0.68	20.74	0.65	−4.56
B－ 6	8.80	31.27	56.82	0.31	2.00	23.14	0.74	19.83	0.63	−14.30
B－ 7	8.80	30.91	56.82	0.31	2.00	23.18	0.75	19.66	0.64	−15.19
B－ 8	8.80	30.21	56.82	0.38	2.00	20.05	0.73	18.52	0.61	−7.63
B－ 9	8.80	32.11	56.82	0.61	2.00	19.59	0.61	17.44	0.54	−10.97
B－10	9.00	28.63	55.56	0.68	2.00	18.04	0.63	15.32	0.54	−15.08
B－11	9.00	25.07	55.56	0.72	2.00	16.80	0.67	13.21	0.53	−21.37
B－12	8.80	30.53	56.82	0.73	2.00	18.32	0.60	15.88	0.52	−13.32
B－13	8.80	30.30	56.82	0.75	2.00	18.18	0.60	15.60	0.52	−14.19
B－14	8.80	30.52	56.82	0.82	2.00	17.70	0.58	15.32	0.50	−13.45
B－15	9.00	25.39	55.56	0.84	2.00	14.98	0.59	12.70	0.50	−15.22
B－16	8.85	25.60	55.50	0.02	5.00	18.03	0.70	19.38	0.76	7.49
B－17	8.95	26.81	55.87	0.06	5.00	18.91	0.70	19.25	0.72	1.80
B－18	8.83	25.28	56.63	0.48	5.00	13.55	0.54	13.15	0.52	−2.95
B－19	8.70	25.55	57.47	0.49	5.00	14.34	0.56	12.85	0.50	−10.39
B－20	8.80	25.55	56.82	0.71	5.00	14.05	0.55	11.27	0.44	−19.79
B－21	8.70	25.55	57.47	0.77	5.00	11.49	0.45	13.29	0.52	15.67
C－ 1	12.80	25.20	39.06	0.00	2.00	24.19	0.96	23.21	0.92	−4.05
C－ 2	12.80	25.09	39.06	0.00	2.00	24.84	0.99	23.13	0.92	−6.88
C－ 3	12.80	25.09	39.06	0.00	2.00	24.59	0.98	23.13	0.92	−5.94
C－ 4	12.80	25.03	39.06	0.00	2.00	25.03	1.00	23.00	0.92	−8.11
C－ 5	12.90	30.16	38.76	0.00	2.00	29.86	0.99	28.14	0.93	−5.76
C－ 6	13.30	29.52	37.59	0.20	2.00	23.91	0.81	24.86	0.84	3.97
C－ 7	13.30	29.51	37.59	0.20	2.00	24.50	0.83	23.81	0.81	−2.82
C－ 8	12.90	30.46	38.76	0.25	2.00	24.67	0.81	24.25	0.80	−1.70
C－ 9	13.30	29.34	37.59	0.26	2.00	24.06	0.82	23.56	0.80	−2.08
C－10	12.91	30.32	38.76	0.36	2.00	24.56	0.81	22.25	0.73	−9.41
C－11	13.30	29.47	37.59	0.42	2.00	21.80	0.74	20.95	0.71	−3.90
C－12	12.90	30.49	38.76	0.43	2.00	23.78	0.78	21.25	0.70	−10.64
C－13	13.30	29.32	37.59	0.43	2.00	21.11	0.72	20.61	0.70	−2.37
C－14	12.90	30.15	38.76	0.52	2.00	22.31	0.74	19.69	0.65	−11.74
C－15	12.90	30.29	38.76	0.53	2.00	23.02	0.76	19.69	0.65	−14.47

Note : $K = \frac{\sigma_{u)the} - \sigma_{u)exp}}{\sigma_{u)exp}} \times 100(\%)$

(1) Square Plates Subjected to Uniaxial Compression

Ueda et. al.[7] conducted ultimate strength series tests for the welded square plates subjected to uniaxial compression.

Table 1 represents the details of the specimen. Three kinds of plate thickness that are 4.5㎜(A−specimen), 9.0㎜(B-specimen) and 12.7㎜(C-specimen) were treated. The boundary condition of the specimen in the experiment was set to be simply supported.

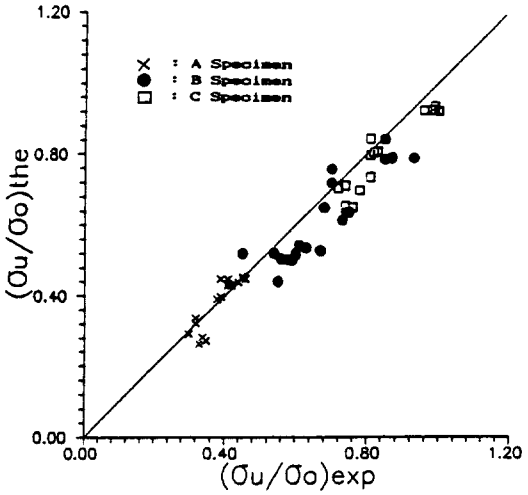

Fig.4 A comparison between the ultimate compressive strengths of square plates obtained by the experiment and present method

Also two kinds of the magnitude of the welding compressive residual stress on which Ueda's measured data is based were assumed in the present analysis described in Table 1. Each specimen is modelled by an idealized plate element and the total numbers of nodal point and the degrees of freedom after the restraint condition is introduced are four.

Table 1 and Fig.4 give the comparison between the ultimate strengths obtained by the experiment and the present analysis. It is clear that the present solution is in good agreement with Ueda's experimental results.

Also since the computing time required in the present analysis was about 20 seconds by using IBM PC/AT computer, the present method is very efficient for the practical use.

(2) Rectangular Plates Subjected to Uniaxial Compression

In order to investigate the influence of the aspect ratio on the ultimate strength of the plate element, elasto-plastic large deflection analysis of initially deflected rectangular plates is performed by applying the nonlinear finite element method developed by the author[8]. These results are then compared with the solution obtained by the present method.

Table 2 indicates the dimensions of the plates.

Table.2 Description of rectangular plates subjected to uniaxial compression

a/b	b (㎜)	t (㎜)	σ_o (kg/㎟)	σ_u (kg㎟) FEM	FEM (10%Up)	Present	Mesh Size in FEM Ana.	W_{om}	CPU Time by CYBER 932/31 for FEM Ana.(Min)
1	500	10	36	27.48	30.23	29.21	5×5	1.0000	23.0
2	500	10	36	30.90	33.99	32.57	10×5	0.0000	45.3
3	500	10	36	28.80	31.68	31.41	15×5	0.3335	72.4
4	500	10	36	29.40	32.34	32.61	20×5	0.0000	103.5
5	500	10	36	29.06	31.97	32.04	25×5	0.2014	141.1

Note : 1) Mesh size in FEM analysis indicates meshes for a quarter plate in the longitudinal and transverse direction

2) W_{om} denotes the magnitude of buckling mode component for the initial deflection

The maximum magnitude of the initial deflection is set to be 10 percent of the plate thickness. The shape of the initial deflection of the rectangular plates was assumed as shown in Fig.6. The configuration of the initial deflection is depicted by Fourier series function using 15 terms as indicated in Fig.5.

As described in section 4.3, the present theory selects only buckling mode component as the deflection parameter. Table 2 gives the buckling mode component of the initial deflection for each plate.

The yield stress of the material is assumed to be 36kg／㎟ and Young's modulus is 21000kg/㎟. The welding residual stress is not present.

In FE analysis, due to the geometric symmetry, a quarter of the plate is modelled. The mesh size number varying aspect ratio is given in Table 2, in which the rectangular plate element having four corner nodal points is employed.

Since the unloading edges of the specimen have no restraints to the in-plane movement, it is expected that the estimated ultimate strength is underestimated by about 10 percent less than the case that the edges remain straight[5]. Thus, Table 2 also compares the ultimate strength that is corrected by adding 10 percent because the idealized plate element was formulated under the consideration that the edges remain straight.

Fig.6 shows the change for the ultimate strength with varying the aspect ratio of the plate. Accuracy of the present solution is sufficient comparing with FEM result. The computing times required in FE analysis by using CYBER 932/31 computer are given in Table 2, while the present analysis needed only 20 seconds by IBM PC/AT computer. It is obvious that the present method is very efficient.

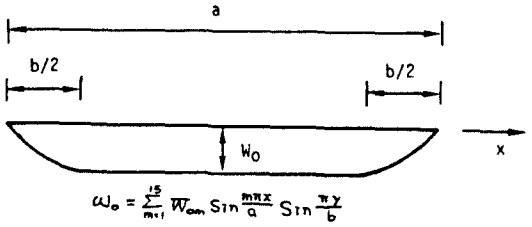

Fig.5 Simplified shape of the initial deflection existing in the plate element

(3) Post-Ultimate Behaviour of the Square Plate Subjected to Uniaxial Compression

In order to verify the accuracy of the present theory in the post-ultimate range, a comparison between the resuts by Kitada's nonlinear FE analysis[9] and the present analysis is made.

Fig.7 represents the load-shortening curve for an imperfect square plate subjected to uniaxial displacement. Solid line indicates Kitada's result and dotted line is present solution.

It is obvious that present method gives an acceptable solution even in the post-ultimate range of the element.

(4) Nonlinear Analysis of Welded Box Column

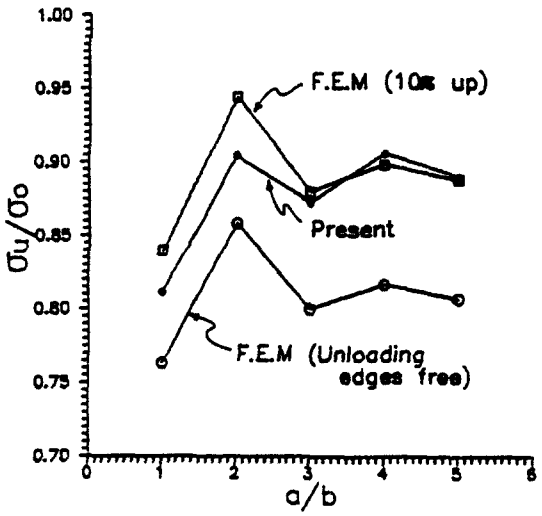

Fig.6 The change of the ultimate strength with varying the aspect ratio of the rectangular plate

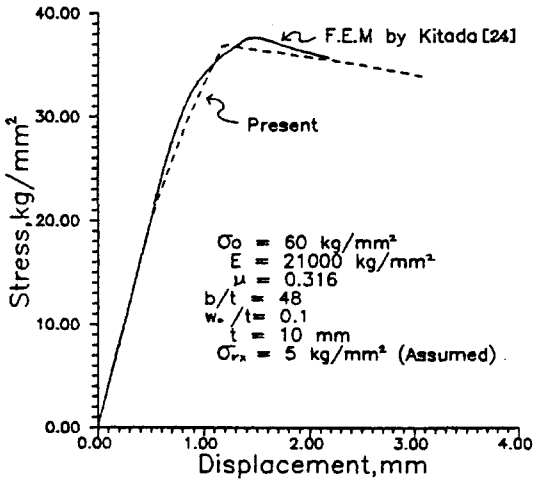

Fig.7 The load−shortening curve for an imperfect square plate subjected to uniaxial displacement

Usami et. al [10] conducted ultimate strength series tests for welded box columns in order to investigate the interaction effect between local and overall buckling of the structure.

Fig.10 shows the configuration of the specimen and their detail demensions are given in Table 3 and 4, in which Table 3 is for shorter specimen and Table 4 is for longer specimen. Among these, S-series indicates that the shape of box section of the specimen is nearly square, while R-series represents the spcimen having the rectangular shape of the scetion. Also, shorter specimen such as S-10 and R-10 series has only end-diaphrams which are attached in both ends of the stucture but longer specimen has two more inside-diaphrams in addition to

Table.3 Description of the test specimen for the shorter welded box column

Specimen No.	B(mm)	D(mm)	t(mm)	L(mm)	EXP		THE		K(%)
					P_u(ton)	P_u/P_p	P_u(ton)	P_u/P_p	
S−10−22	151	127	6.01	501	249.5	0.987	235.5	0.932	−5.6
S−10−27	181	156	6.00	650	264.5	0.865	270.8	0.886	2.4
S−10−33	217	193	6.00	800	280.5	0.753	291.7	0.783	4.0
S−10−38	246	223	6.00	900	280.0	0.657	289.3	0.679	3.3
S−10−44	283	259	6.03	1000	287.0	0.579	303.5	0.612	5.7
R−10−22	151	93.5	5.98	500	235.0	1.063	203.1	0.919	−13.6
							224.6*	1.016*	−4.4
R−10−33	217	144	6.00	700	269.5	0.822	263.1	0.802	−2.4
R−10−44	283	193	6.05	900	283.0	0.649	319.7	0.733	13.0
							301.8*	0.692*	6.6

Note : 1) P_u and P_p denote the ultimate strength and fully plastic strength, respectively

2) Symbols "S" and "R" in specimen number indicate that the shapes of the box section are square and rectangular, respectively

3) Values of initial imperfections measured for typical specimen are σ_r/σ_o=0.087−0.138 (average=0.112) and δ_o/L=0.31−6.29(x10^{-4})

4) Assumed values of initial imperfections used in the present analysis are σ_r/σ_o=0.112, δ_o/L=6.29x10^{-4} and w_o/t=0.1

5) Value marked by asterisk(*) was calculated under consideration of no residual stress and no initial deflection

6) $K=\dfrac{P_{U)\ the}-P_{U)exp}}{P_{U)exp}}\times 100(\%)$

end-diaphrams as shown in Fig.8.

Each plate element is modelled by an idealized plate element. Here, diaphram is also modelled by an idealized plate element. As shown in Fig.8, the end-diaphram is located slightly inside from both ends and for the simplicity of the modelling the plate fragments outside of the end-diaphram is neglected in the present analysis. The boundary and loading condition are also shown in Fig.8. The loading is applied by a displacement control.

A comparison between the ultimate strengths obtained by experiment and present analysis is made in Table 3, 4 and Fig.9. The present solution is in good agreement with the experimental result and the nonlinear behaviour obtained by the present analysis is also acceptable. The computing time required in the present analysis was about 30 seconds to 5 minutes by using CYBER 932/31 computer.

Table.4 Description of the test specimen for the longer welded box column

Specimen No.	B(mm)	D(mm)	t(mm)	L(mm)	EXP		THE		K(%)
					P_u(ton)	P_u/P_p	P_u(ton)	P_u/P_p	
S-35-22	151	127	6.00	1880	215.5	0.852	206.5	0.816	-4.2
S-35-27	182	157	6.02	2310	-	-	238.1		
S-35-33	216	193	6.03	2830	269.5	0.722	254.0	0.680	-5.8
S-35-38	247	223	6.01	3260	265.5	0.621	262.8	0.615	-1.0
S-35-44	283	259	6.01	3770	268.5	0.544	273.9	0.555	2.0
S-50-22	151	122	6.01	2690	183.5	0.740	201.9	0.814	10.0
S-50-27	181	157	6.00	3300	206.5	0.672	236.9	0.771	14.7
S-50-33	217	192	6.00	4040	249.0	0.670	264.6	0.712	6.3
R-50-22	151	94.2	6.00	2090	165.5	0.743	185.4	0.832	12.0
R-50-27	181	116	6.00	2570	197.0	0.731	207.8	0.772	5.5
R-50-33	217	144	6.00	3140	232.5	0.709	233.4	0.712	0.4
R-50-38	247	166	6.00	3610	240.0	0.639	255.1	0.679	6.3
R-50-44	283	193	6.01	4180	250.5	0.579	270.2	0.624	7.9
R-65-22	151	94.4	6.01	2720	132.5	0.593	185.5	0.830	40.0
							157.8*	0.706*	19.1
R-65-27	181	116	6.00	3340	171.5	0.637	211.5	0.785	23.3
							178.8*	0.664*	4.3
R-65-33	217	143	6.00	4080	191.5	0.585	236.5	0.722	23.5
							198.1*	0.605*	3.4

Note : 1) P_U and P_P denote the ultimate strength and fully plastic strength, respectively

2) Symbols "S" and "R" in specimen number indicate that the shapes of the box section are square and rectangular, respectively

3) Values of initial imperfections measured for typical spectimen are $\sigma_r/\sigma_o=0.087=0.138$ (average-0.112) and $\delta_o/L=0.31-6.29(x10^{-4})$

4) Assumed values of initial imperfections used in the present analysis are $\sigma_r/\sigma_o=0.112$, $\delta_o/L=6.29x10^{-4}$ and $w_o/t=0.2$

5) Calculated values marked by asterisk(*) were obtained under the consideration of $\sigma_r/\sigma_o=0.2$, $\delta_o/L=6.29x10^{-4}$ and $w_o/t=0.3$

6) $K=\frac{P_{U)the}-P_{U)exp}}{U)exp}\times 100(\%)$

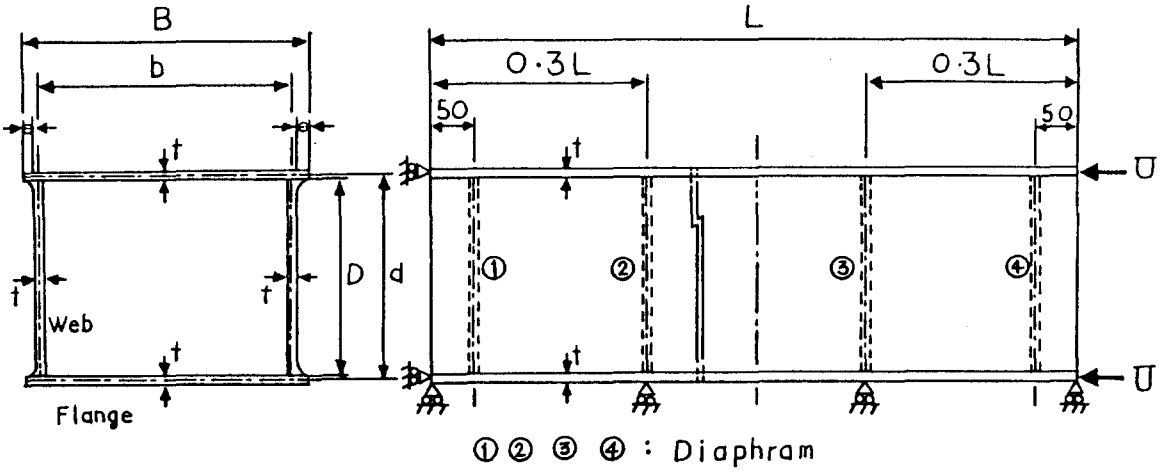

Fig.8 Configuration of the welded box column and its boundary and loading condition

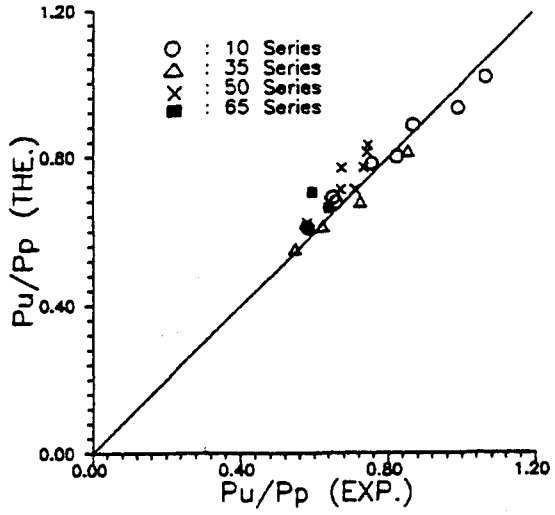

Fig.9 A comparison between the ultimate strengths of the welded box column obtained by the experiment and present method

5. Application to the Double Skin Upper Deck Structure of Product Oil Carrier

The present safety and reliability assessment procedure is applied to the upper deck structure of the double skin product oil carrier designed by Okamoto et. al. [2].

Table 5 represent the principal dimensions. The ABS rule requirement for section modulus is satisfied for the present design as indicated in Table 5.

For simplicity, 32HT material that the yield stress σ_o=32kg/mm^2 and Young's modulus E= 21000kg/mm^2 is used for all structural members. The part of the upper deck structure is modelled by the idealized plate elements formulated in the present study, in which the longitudinal girder is considered to have no stiffeners. The boundary and loading condition is indicated in Fig.10.

In order to investigate the influence of the initial imrerfections and the yield stress on the safety and reliability of the structure, parametric studies are conducted with varying the value of the initial deflection, welding residual stress and the yield stress. Table 6 describes the details of series analysis for the objective upper deck structure. Here, when changing the yield stress of the material, the plate thickness of the element is also changed applying the procedure used in the shipyards. For 24MS material where the yield stress σ_o=

Table 5. Principal particulars of the present double skin product oil carrier

L (m)	B (m)	D (m)	d (m)	C_b	DWT (ton)	Material	SM_d x10^3 (mm^2－m)	SM_b x10^3 (mm^2－m)	SM_{req} x10^3 (mm^2－m)
180.0	32.2	19.5	12.0	0.765	40,000	32HT	19900.2	24824.5	11587.6

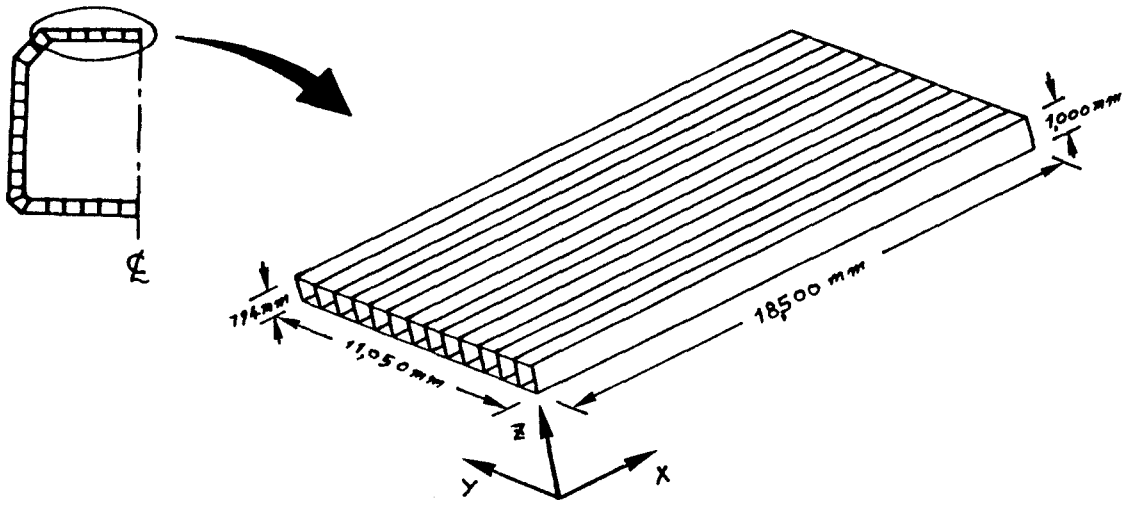

Fig.10.a The ISUM modeling of the double skin deck structure

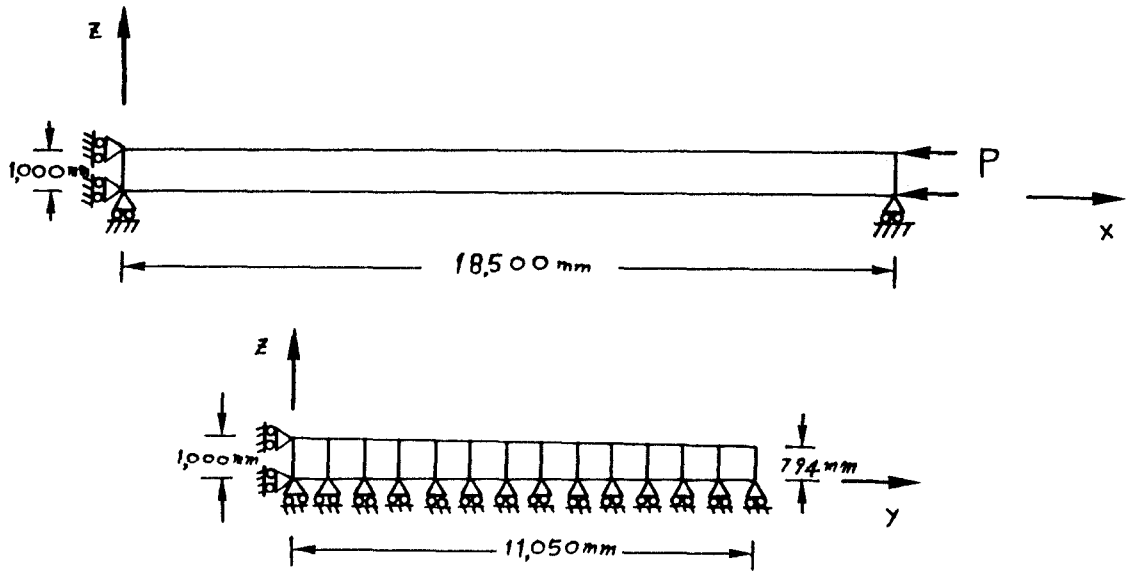

Fig.10.b Outline of the boundary and loading condition used in the present analysis

24kg/mm², the plate thickness becomes to be increased rather than that of 32HT material, that is, $t_{24}=t_{32}/0.78$, in which t_{24} and t_{32} denote the plate thickness for the material of 24MS and 32HT, respectively. Also, for 36HT with $\sigma_o=36$kg/mm², t_{36} which denote the plate thickness for 36HT material becomes to be 0.72/0.78 t_{32}.

Figs.11,12 and 13 indicate the nonlinear behavior of the objective structure representing the influence of the initial deflection, welding residual stress and yield stress, respectively.

Table 7 represents the safety factor and reliability index calculated on the basis of the present procedure described in section 3.

Table.6 Details of series analysis for the upper deck structure

Model	W_0/t	σ_r/σ_o	σ_o(kg/mm²)
S−1	0.01	0.0	32 [2]
S−2	0.1	0.0	32
S−3	0.2	0.0	32
S−4	0.1	0.1	32
S−5	0.1	0.2	32
S−6	0.1	0.1	24 [3]
S−7	0.1	0.1	36 [4]

Note : 1) Residual stress in the longitudinal direction is considered in the present analysis
2) 32kg/mm² denotes the high−tensile steel
3) 24kg/mm² denotes the mild steel
4) 36kg/mm² denotes the high−tensile steel

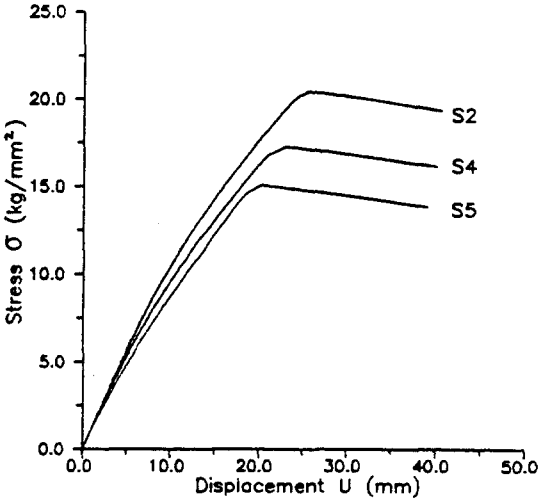

Fig.12 The influence of the residual stress on the ultimate compressive stress of the double skin deck structure

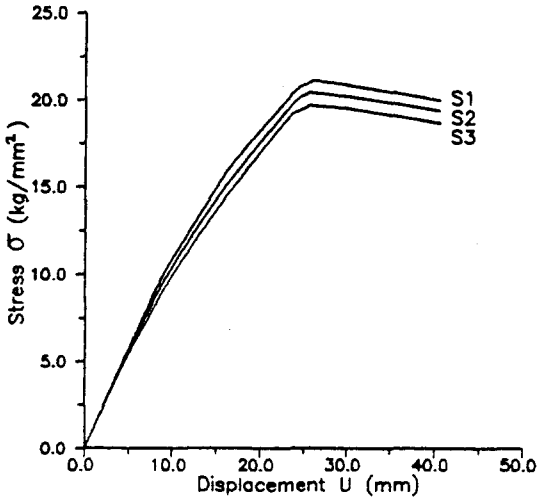

Fig.11 The influence of the initial deflection on the ultimate compressive stress of the double skin deck structure

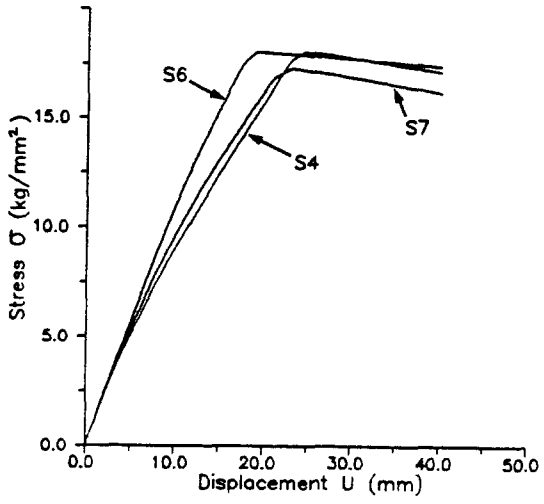

Fig.13 The influence of the yield stress on the ultimate compressive stress of the double skin deck structure

From these results, it is observed that safety factor and reliability index considerably decrease with the increasing of the welding residual stress, and the initial deflection. Also, by applying the high tensile steel plate for the structural member, the level of the safety factor and reliability index is decreased. It may be due to the earlier occurence of the buckling as a result of the reduction of the plat thickness. Therefore, particular attention should be paid when the reduction of the plate thickness is made by employing the high tensile steel plate.

The central safety factor is in the range of 1. 9 and 2.8 and the reliability index is in the range of 4.4 and 6.0. For the existing ship's upper deck structure of oil tanker[11], since the safety factor and reliability index were about 2 and 4, respectivly, the present upper deck structure is considered to have sufficient safety and reliability.

The computing time required in the present analysis about 1 hours by using IBM PC/AT computer.

6. Concluding Remarks

In the present study, a practical safety and reliability assessment procedure for the double skin upper deck structure on the basis of the ultimate compressive strength is proposed.

The theoretical background of the ultimate strength analysis method is placed on the idealized structural unit method. An efficient and accurate mechanical model for the plate element subjected to uniaxial load is formulated taking account of the initial imperfections as well as the interaction effect between the local and global buckling in the structure. The external stress acting on the structure which is due to the still water and wave-induced sagging moment is approximately estimated by using the ABS rule.

The central safety factor is evaluated dividing the ultimate stress by the average value of the external stress. Also the reliability index is estimated by using Cornel's MVFOSM method.

The present procedure is then applied to the safety and reliability assessment of the upper deck structure of the double skin product oil carrier.

From the results of the safety and reliability assessment, it is observed that the welding residual stress and initial deflection reduce the safety and reliability of the structure, Also, when using the high tensile steel material, the earlier occurence of the buckling due to the reduction of the plate thickness should be checked. It is concluded that the present procedure is quite useful for the safety and

Table. 7 The results of safety and reliability assessment for the double skin deck structure

Model	μ_u	μ_s	μ_w	S_u	S_s	S_w	γ	β
S－1	21.11	3.298	4.794	2.111	0.330	0.324	2.609	6.024
S－2	20.43	3.298	4.794	2.043	0.330	0.324	2.525	5.890
S－3	19.69	3.298	4.794	1.969	0.330	0.324	2.433	5.734
S－4	17.27	3.298	4.794	1.727	0.330	0.324	2.134	5.134
S－5	15.08	3.298	4.794	1.508	0.330	0.324	1.864	4.430
S－6	18.02	2.667	3.877	1.802	0.267	0.267	2.754	6.236
S－7	18.02	3.600	5.233	1.802	0.360	0.353	2.040	4.910

Note : $\mu_e=\mu_s+\mu_w$

reliability assessment of the structure like the double skin upper deck structure.

In order to conduct a more reasonable safety and reliability assessment of the ship structure, it is recommended that much attempts to collect data of the central safety factor and the reliability index for existing ship structures which are considered to have sufficient safety and reliability should be performed by using the efficient method such as the present procedure in the sense of the comparative strength concept.

References

[1] N. "A. Cornel, "A Probability-Based Structural Code, J. of American Concrete Institute". Vol. 66, No. 12, 1979.

[2] T. Okamoto et. al., "Strength Evaluation of Novel Unidirectional-Girder-System Product Oil Carrier by Reliability Analysis, Trans". SNAME, 1985.

[3] D. K. Hart et. al., "Structural Reliability Analysis of Stiffened Panels", RINA, 1985.

[4] ABS, Rules for Building and Classing Steel Vessels, 1987.

[5] Y. Ueda, S. M. H. Rashed and J. K. Paik, "Plate and Stiffened Plate Units of the Idealized Structural Unit Method(1st Report)-Under In-Plane Loading", J. of SNAJ, Vol. 156, 1984.

[6] Y. Ueda, S. M. H. Rashed and J. K. Paik, "Effective Width of Rectangular Plates Subjected to Combined Loads", J. of SNAJ, Vol. 159, 1986.

[7] Y. Ueda et. al., "Ultimate Strength of Square Plates Subjected to Compression (1st Report)-Effects of Initial Deflection and Welding Residual Stresses", J. of SNAJ, Vol. 137, 1975.

[8] J. K. Paik and C. Y. Kim, "A Simplified Finite Element Method for the Ultimate Strength Analysis of Plates with Initial Imperfections", J. of SNAK, Vol. 26, No. 1, 1989.

[9] H. Kitada, "A Study on the Ultimate Strength of Plates and Stiffened Plates Subjected to Axial Compression", Dr. Dissertation, Osaka University, Japan, 1980.

[10] T. Usami et. al., "Tests on the Interaction Strength Between Local and Overall Buckling of Welded Box Columns", JSCE, Vol. 308, 1981.

[11] J. K. Paik, "Ultimate Strength-Based Reliability Assessment of Upper Deck Structures", Proceeding of Spring Symposium of SNAK, 1990.